Annals of Biomedical Engineering, Vol. 41, No. 10, October 2013 (© 2013) pp. 2077–2087
DOI: 10.1007/s10439-013-0822-6

BMES BIOMEDICAL ENGINEERING SOCIETY™ www.bmes.org

An Integrated System for 3D Hip Joint Reconstruction from 2D X-rays: A Preliminary Validation Study

STEFFEN SCHUMANN,[1] LI LIU,[1] MORITZ TANNAST,[2] MATHIAS BERGMANN,[3] LUTZ-P. NOLTE,[1] and GUOYAN ZHENG[1]

[1]Institute for Surgical Technology and Biomechanics (ISTB), University of Bern, Stauffacherstr. 78, 3014 Bern, Switzerland; [2]Orthopedic Department, Inselspital, University of Bern, Bern, Switzerland; and [3]Institute of Anatomy, University of Bern, Bern, Switzerland

(*Received 16 November 2012; accepted 30 April 2013; published online 14 May 2013*)

Associate Editor Sean S. Kohles oversaw the review of this article.

Abstract—The acquisition of conventional X-ray radiographs remains the standard imaging procedure for the diagnosis of hip-related problems. However, recent studies demonstrated the benefit of using three-dimensional (3D) surface models in the clinical routine. 3D surface models of the hip joint are useful for assessing the dynamic range of motion in order to identify possible pathologies such as femoroacetabular impingement. In this paper, we present an integrated system which consists of X-ray radiograph calibration and subsequent 2D/3D hip joint reconstruction for diagnosis and planning of hip-related problems. A mobile phantom with two different sizes of fiducials was developed for X-ray radiograph calibration, which can be robustly detected within the images. On the basis of the calibrated X-ray images, a 3D reconstruction method of the acetabulum was developed and applied together with existing techniques to reconstruct a 3D surface model of the hip joint. X-ray radiographs of dry cadaveric hip bones and one cadaveric specimen with soft tissue were used to prove the robustness of the developed fiducial detection algorithm. Computed tomography scans of the cadaveric bones were used to validate the accuracy of the integrated system. The fiducial detection sensitivity was in the same range for both sizes of fiducials. While the detection sensitivity was 97.96% for the large fiducials, it was 97.62% for the small fiducials. The acetabulum and the proximal femur were reconstructed with a mean surface distance error of 1.06 and 1.01 mm, respectively. The results for fiducial detection sensitivity and 3D surface reconstruction demonstrated the capability of the integrated system for 3D hip joint reconstruction from 2D calibrated X-ray radiographs.

Keywords—X-ray image, Calibration, Statistical shape model, 3D surface model, Proximal femur, Pelvis.

Address correspondence to Steffen Schumann and Guoyan Zheng, Institute for Surgical Technology and Biomechanics (ISTB), University of Bern, Stauffacherstr. 78, 3014 Bern, Switzerland. Electronic mails: steffen.schumann@ieee.org, guoyan.zheng@ieee.org

INTRODUCTION

Despite the latest technological advancements, conventional X-ray image acquisition remains the standard imaging procedure for orthopedic interventions. Although planar X-ray radiographs provide only two-dimensional (2D) information and are therefore difficult to interpret correctly, it is commonly available, reasonably inexpensive and exposes the patient to only low radiation. For the diagnosis of femoroacetabular impingement (FAI), an anterior–posterior (AP) and an oblique X-ray image are conventionally acquired preoperatively.[5,20] Recently, several studies have shown the great advantage of using three-dimensional (3D) surface models to diagnose orthopedic impairments such as tibial plateau fractures,[22] scoliotic spine deformities,[12] or FAI.[19] In order to analyze potential bony conflicts between acetabular structures of the pelvis and the proximal femur, the hip joint range of motion (ROM) could be dynamically assessed by observation of the relative motion of pelvic and femoral surface models.[9,18]

3D surface models are normally generated by segmentation of 3D datasets from imaging modalities such as computed tomography (CT) or magnetic resonance imaging (MRI). While CT-scans are only acquired in rare cases of severe pelvic deformations,[4] the segmentation of bones from MRI data poses a challenge to the surgeon. Since X-ray radiographs are routinely acquired for diagnosis and planning of FAI, a 2D/3D hip joint reconstruction would be desirable.

3D reconstructions with focus on the acetabular regions have not been reported so far. Existing work mainly focused on the reconstruction of the global pelvic shape.[10,14,23,24] Lamecker *et al.*[10] proposed to

register a thickness image of a pelvis statistical shape model (SSM) to silhouettes, previously extracted from the X-ray image. Validation was performed on 23 digitally reconstructed radiographs (DRRs) datasets. Sadowsky *et al.*[14] proposed a method, which abandons the extraction of pelvic contours. They registered a joint statistical shape and intensity atlas to simulated fluoroscopic images based on normalized mutual information. Solely a single X-ray radiograph was used to reconstruct the 3D shape of the pelvis by Zheng.[24] The resulting scaled surface model is used to measure the post-operative cup orientation in terms of anteversion and inclination angle. Yao and Taylor[23] developed a deformable 2D/3D registration method between DRRs and a hemi-pelvis SSM, constructed from eight training instances. The method was tested with images, synthetically generated from CT scans.

In previous work we have successfully demonstrated the 3D surface reconstruction of the proximal femur from two X-ray radiographs.[17,25] The X-ray images were calibrated using a bulky biplanar calibration device, which however was impractical for the clinical routine. Therefore, the first goal of the present study is to develop and validate a new smaller sized calibration phantom, which can be seamlessly integrated into the X-ray imaging process. It contains only few fiducials and can be easily placed next to the anatomy of interest. Moreover, we extended the 2D/3D reconstruction approach to the acetabular region. As special attention has to be paid to correctly reconstruct the correct fossa depth and rim curvatures of the acetabulum, the second goal of the present study is to develop and validate a new method using the patch statistical shape model (patch-SSM) concept to reconstruct the 3D shape of the acetabulum from biplanar radiographs. Finally, based on these two new developments and the 2D/3D reconstruction of the proximal femur that we have done before, the third goal of the present study is to develop and validate an integrated system for reconstructing 3D hip joints from 2D X-ray images. This paper extends our previous work presented at the International Conference on Information Processing in Computer Assisted Interventions[16] by proposing a more robust and fully automatic calibration phantom detection pipeline and by integrating the 2D/3D reconstruction of the proximal femur as part of the whole system. In order to validate the developed system, X-ray radiographs of dry cadaveric bones and a cadaveric specimen with soft tissue were accordingly acquired and calibrated. We measured the fiducial detection sensitivity and analyzed the reconstruction accuracy by comparison with ground truth 3D models derived from CT-scans. The trial on the cadaveric specimen with soft tissue was conducted in order to prove the feasibility for future clinical usage.

MATERIALS AND METHODS

X-ray Calibration Phantom

Although conventional X-ray imaging is routinely used in clinics, scaling information is normally not available. In order to facilitate quantitative measurements and to determine the spatial relationship between a number of radiographs, image calibration is required. This step is normally performed by integrating a calibration object of known geometry into the imaging process. By establishing correspondences between points $\boldsymbol{X}_i$ in 3D space and their associated 2D projections x_i, the intrinsic and extrinsic calibration parameters can be computed for instance using direct linear transformation (DLT).[1] Thereby, the X-ray image acquisition can be modeled as a finite projective camera[7]:

$$P = KR\left[I\middle|-\tilde{C}\right] \tag{1}$$

where P is the camera projection matrix, K is the intrinsic calibration matrix, and I is the identity matrix. R and $\tilde{C}$ describe the extrinsic calibration parameters in terms of camera orientation and position, respectively. The main task of a calibration procedure is to compute the camera projection matrix P. This can be achieved by DLT, which has the advantage that only linear equations need to be solved for the camera projection matrix. Given a number of point correspondences between 3D points $X_i = [\,X_i \quad Y_i Z_i \quad 1\,]^{\mathrm{T}}$ and 2D points $x_i = [\,u_i \quad v_i \quad 1\,]^{\mathrm{T}}$, P needs to be determined, such that

$$x_i = P \cdot X_i \tag{2}$$

For the purpose of X-ray radiograph calibration, a special calibration object was developed. This mobile calibration phantom (see Fig. 1) is made out of radiolucent plastic material containing radiopaque steel fiducials. In total 16 spherical fiducials of two different sizes are embedded. Seven large fiducials are distributed in one plane and arranged in three unique line patterns $M_i^1, M_i^2, M_i^3, i = 1, 2, 3$ (see Fig. 1, right). Moreover, nine small fiducials are distributed over another two planes. For a successful calibration, at least one of the three unique line patterns of large fiducials with different ratios $r_i = |M_i^1 M_i^2|/|M_i^2 M_i^3|$ needs to be identified based on the 2D projection of the phantom.

X-ray Phantom Detection

In order to establish the required correspondences for calibration, the 2D fiducial positions need to be detected in the X-ray images and assigned to the corresponding 3D coordinates. The fiducial detection is

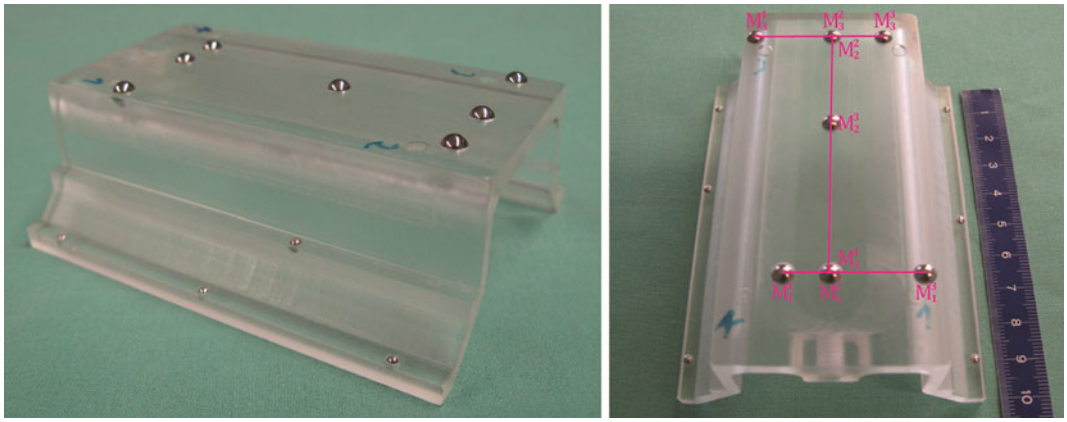

FIGURE 1. Side and top view of the mobile calibration phantom.

thereby constrained to a region-of-interest (ROI), which is interactively determined by picking four points within the image. The extracted ROI is depicted in Fig. 2a. In order to identify possible fiducial candidates, we apply a sequence of image processing steps. In the first place we enhance the contrast of the image using contrast limited adaptive histogram equalization (CLAHE). The CLAHE algorithm has been developed by Pizer *et al.*[13] and is based on the adaptive histogram equalization (AHE). AHE improves the image contrast by performing histogram equalization mapping for each pixel, taking the surrounding pixels into account. Since also noise is enhanced, CLAHE algorithm applies limited contrast enhancement by restricting the slope of the mapping function. Thereby, the local contrast of the image is improved, whereas the noise in homogeneous regions is only slightly amplified. We apply the CLAHE algorithm to the ROI based on the implementation of Heckbert.[8] An exemplary output of CLAHE algorithm is depicted in Fig. 2b. Due to the high density of the steel fiducials, they appear as bright spots within the image and can be further highlighted by mapping the image to larger grayscales (see Fig. 2c). Circular Hough transformation (CHT)[6] is then applied to the output of the intensity mapping in order to determine circular shapes. As the X-ray image acquisition is normally a standardized procedure, an interval of potential circle radii can be estimated based on the pixel spacing, the actual fiducial diameter, and the film-focus distance.

The fiducial candidates of the initial detection stage are further processed in order to filter out possible outliers and to establish correspondences with the 3D coordinates using a simulation-based approach. As already indicated, the detection of three collinear large fiducials is needed for a successful phantom detection. Therefore all large fiducial candidates of the initial detection stage are further examined with respect to collinearity. Subsequently, the ratio of the distances between three collinear candidates is further compared with the technical specifications. If a match with a certain precision could not be found, the phantom detection process is regarded as failed. However, if a triple of collinear large fiducials matches the specification, image normalization is performed. Based on the identified three large fiducials, a local coordinate-system (COS) is established and the set of fiducial candidates (including possible outliers) is normalized with respect to this COS. Due to this normalization step, the original seven degrees of freedom (three for rotation, three for translation, and one for scaling in viewing direction of the X-ray camera) are reduced to two degrees. The scaling, translation, and one rotational component (here: R_z) around the viewing axis (here: z-axis) are canceled out by the normalization step.[15]

In order to identify valid fiducial candidates, the normalized detections were matched with a look-up table (LUT), containing simulated fiducial projections in normalized space. For this purpose, an X-ray image of the calibration phantom in neutral position has been acquired. After establishing correspondences between 2D projections x_i^{ref} and 3D fiducial coordinates X_i^{ref}, the projection matrix P^{ref} and the extrinsic parameters R^{ref} and C^{ref} were computed. Based on the assumption that the intrinsic calibration matrix K^{ref} remains constant between two images, any other X-ray projection can be modeled as follows:

$$x_i = K^{\text{ref}} \cdot \left[R^{\text{ref}} \cdot \left(R^x R^y R^z \cdot X_i - \tilde{C}\right) - \tilde{C}^{\text{ref}}\right] \quad (3)$$

where R_x, R_y, R_z represent the rotation matrix around a particular axis (z-axis in imaging direction) and $\tilde{C}$ the translation between the actual and the reference position. For each LUT entry the 3D fiducial coordinates X_i^{ref} were projected onto the image using the intrinsic calibration matrix K^{ref} and various combinations of the extrinsic rotational components (R_x and R_y).

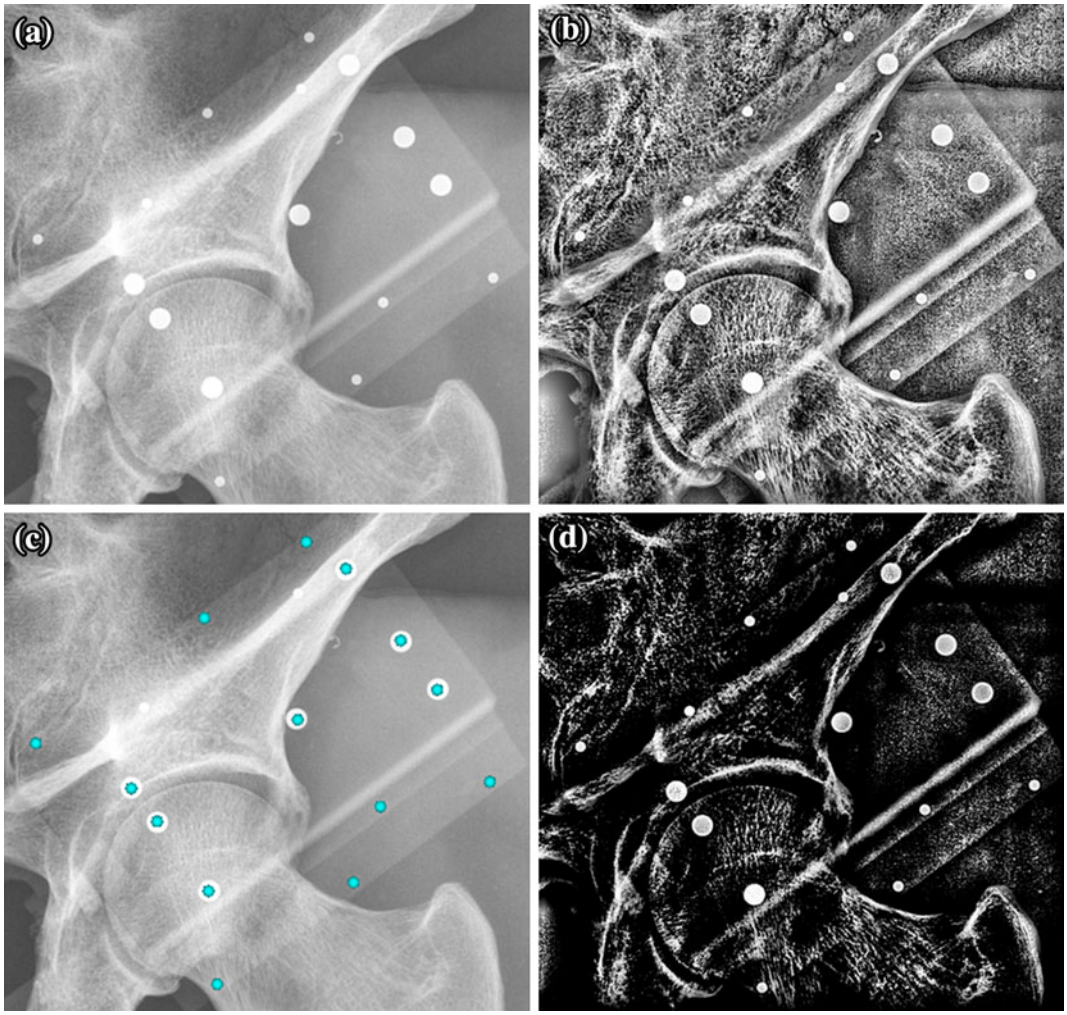

FIGURE 2. Different stages of calibration phantom detection: (a) extracted region of interest; (b) contrast enhanced image using CLAHE algorithm; (c) output of intensity mapping; (d) final detected phantom fiducials.

The optimal LUT item is identified by computing the probability between each LUT item and the set of normalized detected fiducial candidates. Therefore, one distance map is generated for each fiducial type based on the coordinates of the detected fiducial candidates. The probability of each LUT item is then computed based on the Euclidean distance between the simulated projections of this particular LUT item and the two distance maps. The projection coordinates of the LUT item with highest probability are then re-normalized and projected onto the X-ray image. Normalized cross-correlation[11] is further applied to identify the precise fiducial positions (see Fig. 2d). Thereby, the search space is constrained to the neighborhood of the LUT estimated fiducial positions. As correspondences between 2D and 3D fiducial positions are inherently established *via* the LUT, DLT could be applied to determine the final camera projection matrix P.

3D Hip Joint Reconstruction

In our previous work we proposed a method for 3D reconstruction of the proximal femur from two calibrated X-ray radiographs.[25] A SSM of the proximal femur was constructed and registered to the X-ray space using semi-automatically extracted contour information of the proximal femur. This step was followed by a statistical instantiation and non-rigid deformation of the SSM to reconstruct the patient-specific shape of the proximal femur. For details of the 3-stage approach we refer to our previous work.[25]

However, the same approach could not be directly applied to the pelvis. As we are mainly interested in the local acetabular region, a global registration approach of a pelvis SSM might not reveal the precise fossa depth and rim curvatures. Therefore, we recently developed a hierarchical strategy (see Fig. 3) to

precisely reconstruct the shape of the acetabulum.[16] The basic concept relies on the registration of two different SSMs. The first SSM is constructed from CT-segmented surface models of the hemi-pelvis (both patient sides). Correspondence between the surface models is established using diffeomorphic demons algorithm[21] and the statistical variability is explored using principal component analysis (PCA). The second SSM is constructed on the basis of the hemi-pelvis SSM. The mean hemi-pelvis model is used to interactively define the acetabulum region. As correspondence between the hemi-pelvis surface models is known, an acetabular surface patch could be extracted from each hemi-pelvis instance. The acetabular patch instances are further aligned to the one extracted from the mean hemi-pelvis model in order to capture the local shape variations of the acetabulum. Subsequently, PCA is applied, resulting in an acetabular patch-SSM.[16]

In order to register the SSMs to the X-ray space, the following contours need to be semi-automatically extracted from the X-ray images (see Fig. 4b) using live-wire technique[3]:

- Contour of hemi-pelvis
- Anterior contour of acetabular rim
- Posterior contour of acetabular rim
- Contour of acetabular fossa.

Beyond the contour extraction, three pelvic landmarks [anterior superior iliac spine (ASIS), pubis symphysis and posterior inferior iliac spine (PSIS)] have to be defined on both X-ray images (see Fig. 3, step a). The remaining steps of the hierarchical registration are performed automatically. After extracting the features the hemi-pelvis SSM is registered to the X-ray scene based on the landmark information using paired-point matching (see Fig. 3, step b). The corresponding three landmarks were predefined during the modeling process. In the next step, the 3-stage algorithm is accomplished,[25] consisting of affine registration, instantiation, and non-rigid deformation to achieve an optimal match of the hemi-pelvis SSM with the X-ray scene (see Fig. 3, step c). As the alignment of the hemi-pelvis to the X-ray scene is solely based on the outer contours, the fitting around the acetabular region needs to be further improved. Thus, the hemi-pelvis model is replaced by the acetabular patch-SSM using the previously established correspondence (see Fig. 3, step d). The subsequent registration of the patch-SSM is performed in another three steps. A scaled, rigid registration is computed (see Fig. 3, step e) by matching the 3D apparent contours (silhouettes) of the patch-SSM to the anterior and posterior X-ray contours. It was found that the estimation of the acetabular scale is of major importance for a precise 3D shape reconstruction. In order to derive the scale, the first principal axis is computed for the anterior and posterior acetabular contour sets of the AP- and oblique X-ray image and the patch-SSM. Afterward the contour points are projected onto the respective principal axis and the maximum distance d_{axis} among the projected points is computed for all three sets. The average distance for both X-ray images $d_{\text{axis}}^{\text{AP,axial}}$ is further converted to mm unit by multiplication with the pixel scaling factor (determined by the calibration process). The acetabular scale is then determined out of the ratio between the average image distance $d_{\text{axis}}^{\text{AP,axial}}$ and the patch-SSM distance $d_{\text{axis}}^{\text{patch}}$.

This step is followed by an affine registration by involving the acetabular fossa (see Fig. 3, step f). As the fossa of the acetabular patch-SSM does not have a unique silhouette, correspondences to the X-ray image contours need to be determined iteratively. For each iteration all the image contour points are backprojected, resulting in 3D rays. For each 3D ray, the closest vertex of the mean patch model is determined and taken as corresponding point. Together with the acetabular rim point pairs, an affine transformation is computed and applied to the acetabular patch-SSM until convergence. The 3D reconstruction of the acetabulum is then completed by statistical instantiation (Figs. 3, step g and 4c), resulting in a patient-specific 3D model of the acetabulum.

Experimental Design

In order to evaluate the robustness and accuracy of the fiducial detection and calibration, we carried out two experiments based on biplanar X-ray radiographs. Six pairs of X-ray images (AP and oblique view) of dry cadaveric bones (one pelvis and one femur bone at a time) and one pair of X-ray images of a cadaveric specimen with soft tissue (cut above the pelvis and at half length of femur) were acquired. In order to compensate for potential motion of the dry cadaveric bones during X-ray image acquisition, both bones and the phantom were equipped with passive reference bases and tracked by an infrared camera system (NDI Polaris, Ontario, Canada). In case of the cadaveric specimen with soft tissue, the calibration phantom was attached to the pubis symphysis region using a conventional belt. The calibration phantom in this case acts as a tracking device to get the relative position between two images. No external tracking is used for the case of the cadaveric specimen with soft tissue.

In the first experiment we measured the sensitivity of the fiducial detection at two different stages. The robustness of the fiducial detection was analyzed by computing the sensitivity rate. Thereby, the number of determined fiducials was recorded, which were

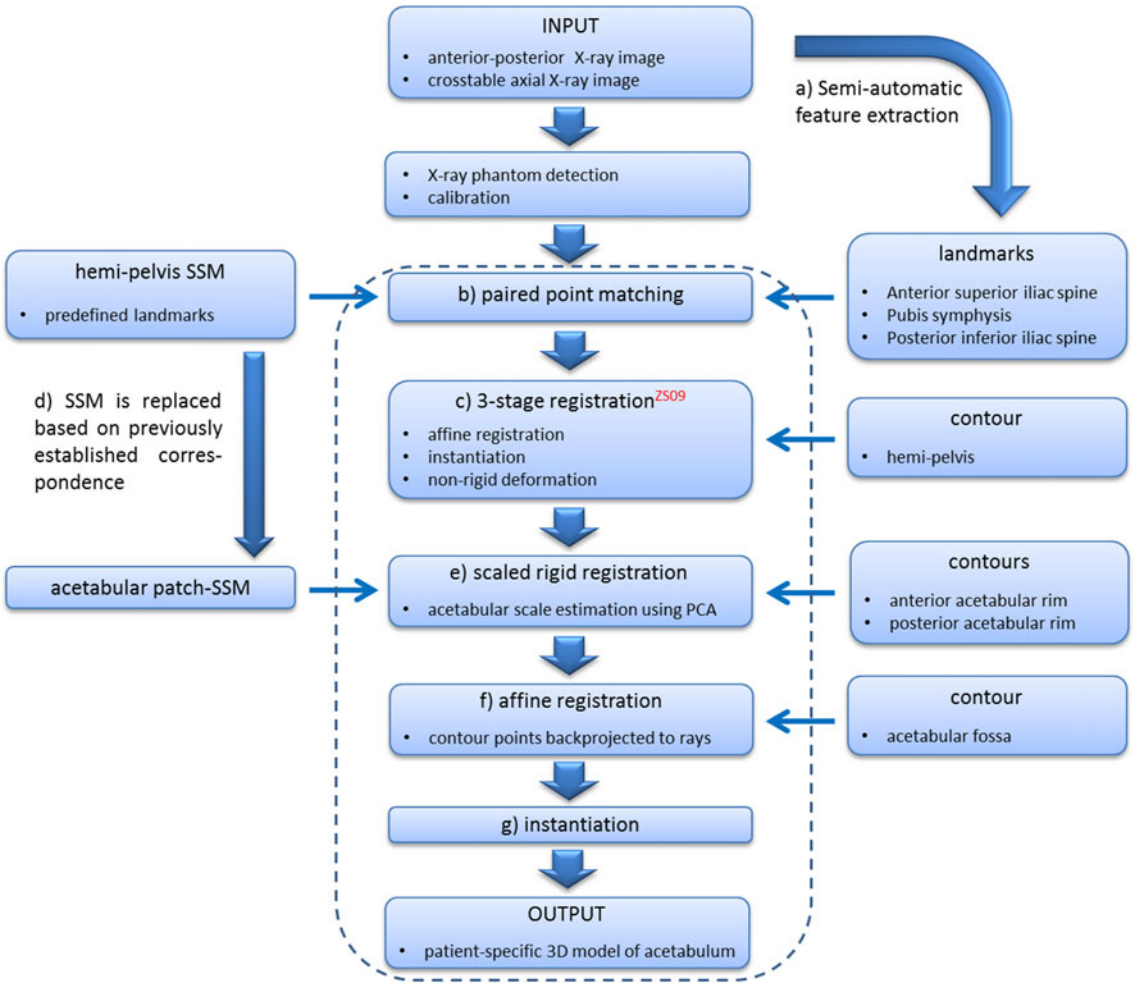

FIGURE 3. Flow chart illustrating the acetabulum reconstruction procedure. See text for details of each step.

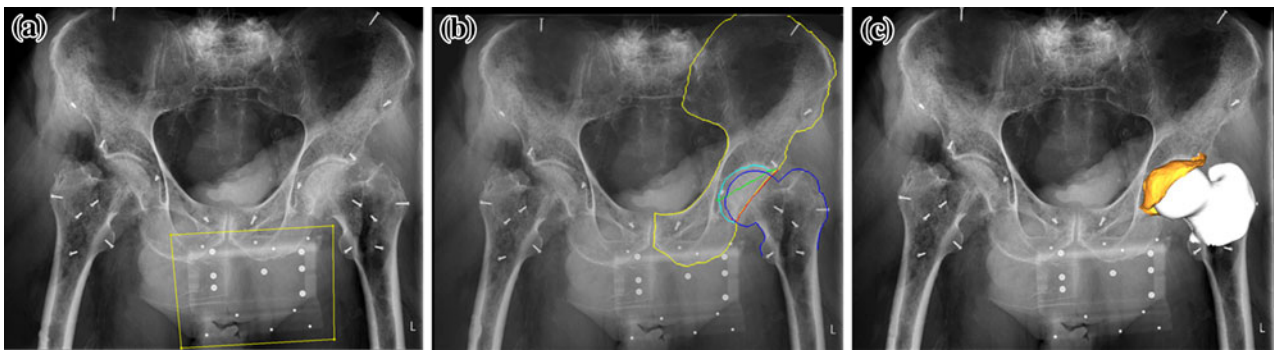

FIGURE 4. Stages of 2D/3D hip joint reconstruction: (a) X-ray radiograph with interactively defined bounding box; (b) defined pelvic and acetabular contours (yellow: contour of hemi-pelvis, blue: contour of proximal femur, green: anterior contour of acetabular rim, red: posterior contour of acetabular rim, cyan: contour of acetabular fossa); (c) 3D reconstructed models of the acetabulum and proximal femur.

correctly identified. This was done for the initial image-based detection (input to simulation-based detection) and for the final LUT-based detection. In total seven biplanar X-ray image datasets (AP and oblique view) of six different pelvic and femoral dry cadaver bones and one cadaveric specimen with soft tissue were available. For each dataset the number of correctly identified fiducials was compared to the total number of visible fiducials, whereas we distinguished between the particular fiducial sizes.

In the second experiment, we calibrated the X-ray radiographs and applied both 2D/3D reconstruction methods, resulting in 3D surface models of the pelvis and proximal femur. For validation, CT-scans of the corresponding hip bones were acquired, segmented, and further served as ground truth. The CT-scan acquisition of the dry bones was performed using Emotion 6 scanner from Siemens (Erlangen, Germany). Always two femur bones were scanned simultaneously (pixel dimensions: 512 × 512 × 800; voxel size: 0.53 mm × 0.53 mm × 0.6 mm; slice thickness: 1.25 mm; current: 100 mA, generator power: 17 kW), while the pelvic bones were scanned individually (pixel dimensions: 512 × 512 × 370; voxel size: 0.59 mm × 0.59 mm × 0.6 mm; slice thickness: 1.25 mm; current: 65 mA, generator power: 8 kW) and the segmentation was semi-automatically performed using Amira software (VSG, FEI Company, Hillsboro, United States of America). For the CT-scan acquisition of the cadaveric specimen with soft tissue a Siemens Somatom Definition Flash device was used (pixel dimensions: 512 × 512 × 441; voxel size: 0.95 mm × 0.95 mm × 1.0 mm; slice thickness: 1.0 mm; current: 42 mA; generator power: 20 kW). While the ground truth proximal femur surfaces could be aligned with the reconstructed models using surface based registration, the ground truth hemi-pelvis surface models had to be further processed: Firstly, the ground truth hemi-pelvis surfaces were non-rigidly registered to the mean hemi-pelvis model using diffeomorphic demons algorithm[21] in order to establish correspondence to the SSM space. Secondly, an acetabulum patch was extracted from the registered hemi-pelvis model and rigidly registered to the reconstructed 3D acetabular model on the basis of direct correspondences.

RESULTS

The numbers of correctly detected fiducials were identified for the initial and LUT-based detection stages and compared to the total number of projected fiducials (see Table 1). The detection results of the datasets marked with an asterisk produced outliers. In dataset '005' one screw head was mistakenly detected, whereas in datasets '002', the initial image-based detection identified three screw heads as fiducials. However, for each case, the wrong detections were eliminated by the subsequent simulation-based step. The overall sensitivity for the initial image-based detection is 95.92% for the large fiducials and 88.09% for the small fiducials. The sensitivity is improved by the final simulation-based detections to 97.96% for the large fiducials and 97.62% for the small fiducials. On average, the initial detection took 1.41 s (1.03–2.13 s), the LUT-based detection 1.01 s (0.99–1.03 s) on a conventional computer (Quad-Core, 3.10 GHz). The dimensions of the image bounding box region were 904 × 865 pixels on average. The SSMs of the proximal femur and pelvis were each constructed from a population of 30 instances, collected from pre-operative CT-scans.

The surface reconstruction accuracy was analyzed using MESH-tool,[2] which compares triangular surface meshes based on the Hausdorff distance. Besides the mean and root mean squared (RMS) distance error, the 5, 25, 50, 75, and 95% percentile errors were computed and plotted as a box plot (see Fig. 5). On average, the acetabulum could be reconstructed with a mean surface distance error of 1.06 ± 0.14 mm, while the error for proximal femur reconstructions was 1.01 ± 0.16 mm. Regions of biggest error occurred either in the fossa region (see Fig. 6, left), or at the cutting edge of the patch (see Fig. 6, right). The computation time of the 3D reconstruction of the acetabulum was 27.79 s on average (22.4–33.18 s). The hip joint of the cadaveric specimen with soft tissue contributed to this result with a mean error of 1.06 mm for the acetabulum reconstruction and a mean error of 0.88 mm for the reconstruction of the proximal femur (see Fig. 7).

The maximum mean error among the seven datasets was 1.25 mm for the acetabulum surface and 1.28 mm for the surface of the proximal femur. Beyond the surface reconstruction error of the acetabulum we explicitly investigated the accuracy of the acetabular rim. Therefore, vertices along the rim were interactively chosen on the basis of the mean acetabulum patch and transferred to the ground truth and reconstructed acetabular surface models (see Fig. 8). By direct comparison of the contour points, an average Euclidean distance error of 1.40 ± 0.27 mm was found.

DISCUSSION AND CONCLUSIONS

3D bone reconstructions from conventional biplanar X-ray images would be an enormous benefit for clinical diagnosis and planning. In order to extract quantitative information from X-ray radiographs, a calibration step is inevitable. However, the integration of a calibration object into the imaging process and the subsequent image-based detection is a complex task.

Therefore, we proposed an integrated system to perform X-ray radiograph calibration and 2D/3D hip joint reconstruction. We developed a mobile calibration phantom, which could be placed next to the anatomy of interest and which did not interfere with the image acquisition. The phantom has sparsely

TABLE 1. Comparison of initial and final fiducial detection stages.

	Initial detection		LUT detection	
Dataset	Large fiducials	Small fiducials	Large fiducials	Small fiducials
001	14/14	16/18	14/14	17/18
002*	14/14	13/18	14/14	18/18
003	12/14	16/18	13/14	17/18
004	12/14	15/18	13/14	18/18
005*	14/14	17/18	14/14	18/18
006	14/14	16/18	14/14	17/18
007	14/14	18/18	14/14	18/18

Datasets 001–006 were acquired from dry cadaveric bones, dataset 007 was acquired from a cadaveric specimen. Datasets marked with an asterisk produced outliers. In both datasets, screws were mistakenly detected as fiducials in the initial detection step, but eliminated by the LUT step.

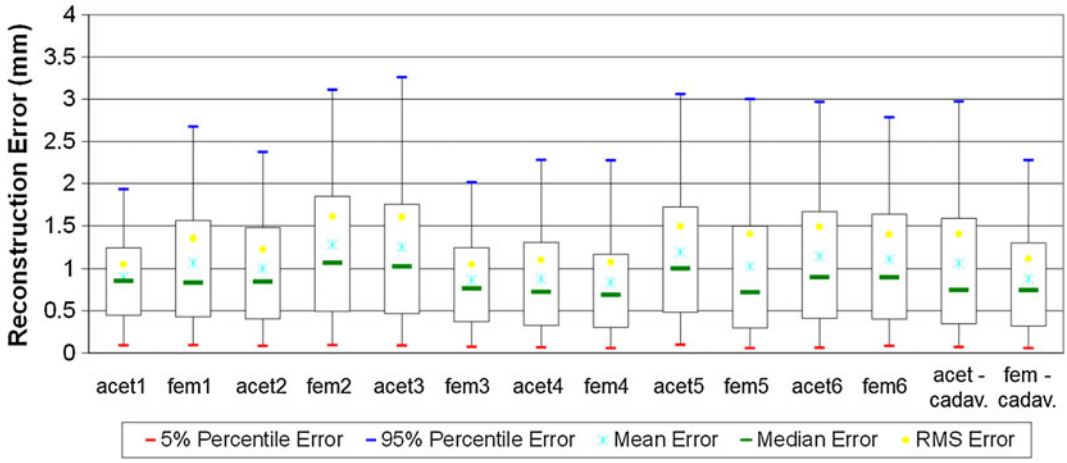

FIGURE 5. Box plot indicating the error distribution of the seven reconstructed hip joint surface models (six dry cadaveric hip bones plus one cadaveric specimen with soft tissue).

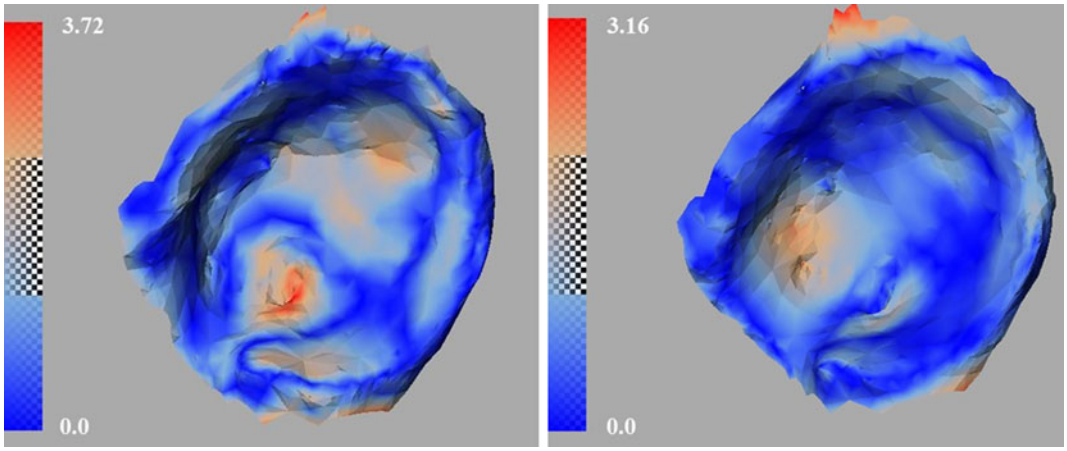

FIGURE 6. Visualization of reconstruction error as superimposed on the reconstructed acetabular surface models.

distributed small fiducials embedded, which are projected onto the X-ray image. In order to extract the projected fiducials in a robust manner, we propose a detection pipeline based on image pre-processing and LUT-based matching. While in the first stage, potential fiducial detections are extracted, outliers are identified and correspondences with the 3D fiducials positions are established in the second stage. Due to the reduced

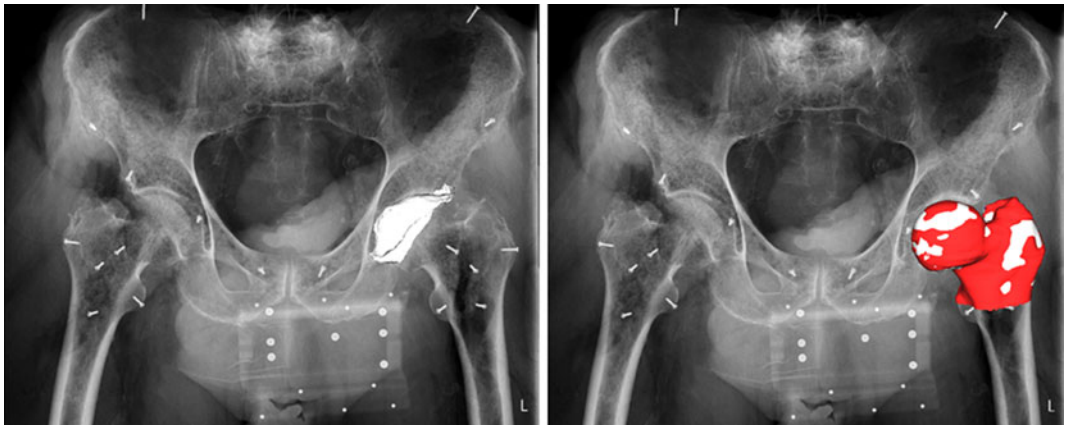

FIGURE 7. Superimposition of the reconstructed models on the AP X-ray image of the cadaveric specimen with soft tissue. The left image shows the superimposed reconstructed acetabulum and the right image shows the reconstructed proximal femur (white) together with the registered ground truth model (red).

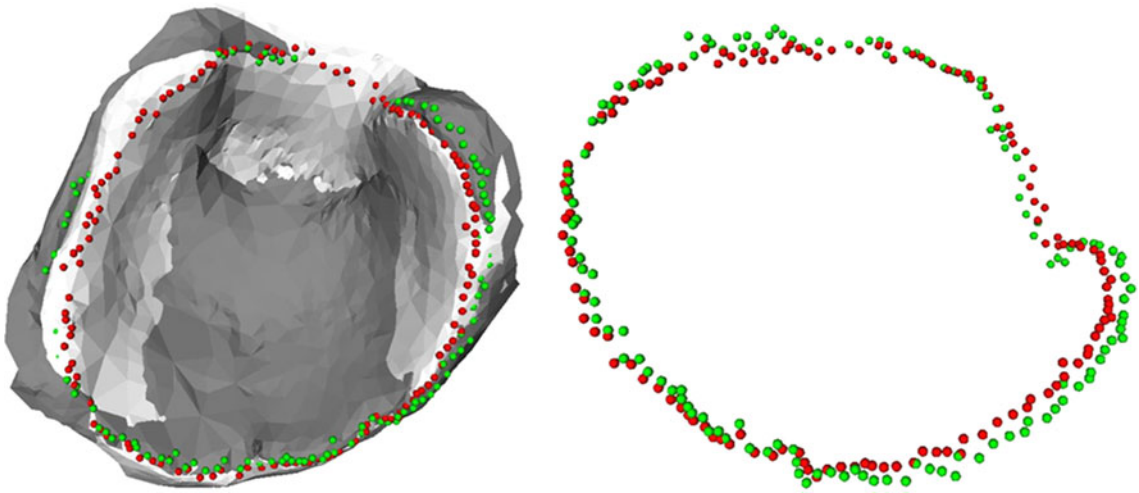

FIGURE 8. Comparison of acetabular rim reconstructions: the rim of the reconstructed model (gray model, green rim contour points) is compared with the ground truth model (white model, red rim contour points).

dimensionality and the small number of fiducials, the whole detection process takes 1–2 s on a conventional computer. The evaluation of seven pairs of X-ray images demonstrated very robust detection results with a sensitivity higher than 95%.

The calibrated X-ray images were further used to reconstruct 3D models of the hip joint. In order to achieve a precise reconstruction of the acetabulum, we proposed a hierarchical registration strategy. The non-rigid registration of the hemi-pelvis SSM to the extracted contours of the X-ray images is used to guide the registration of the localized acetabular patch-SSM. The available X-ray contours of the acetabulum together with the calibration information are then used to optimally reconstruct the shape of the acetabulum. The major shortcoming of the proposed approach is the required user interaction to extract the contours from the X-ray images. However, as a semi-automatic contour extraction method is used, the actual burden is reasonably low.

To validate the hip joint reconstruction, X-ray radiographs of cadaveric bones and a cadaveric specimen with soft tissue were analyzed. In order to compensate for potential motions of the separate dry bones, the phantom and the bones (femur and pelvis) were tracked with an infrared camera system. However, this is not the scenario that we envision in a clinical application. Thus, in order to demonstrate the feasibility for future clinical usage of our approach, we designed and conducted a trial on a cadaveric specimen with soft tissue, where we could rigidly attach the calibration phantom to the cadaveric specimen with a conventional belt. No external tracking was used. The results from this trial showed that our approach, when tested on the cadaveric specimen with soft tissue, could achieve an equivalent accuracy to the dry bone studies.

Since CT scans of two different resolutions were used to establish the ground truth in our validation study, the fact that the errors measured with the coarser-resolution ground truth data (cadaveric specimen with soft tissue) are within the limits of those measured with the finer-resolution ground truth data (dry bones) speaks in favor of the present system.

While accurate, the present approach has limitations. Although we have demonstrated that we could rigidly attach the calibration phantom to the cadaveric specimen with soft tissue using a conventional belt and then use the phantom as a tracking device, it may pose a challenge when we try to rigidly fix the calibration phantom to a patient in a future clinical trial. We are currently revising the design of the phantom by taking the shape of a target anatomy into consideration such that this newly designed calibration phantom can be adapted to the shape of the target anatomy. The second limitation is due to the semi-automatic contour extraction. Our experimental results showed that the live-wire based semi-automatic contour extraction worked well for dry bones as well as for cadaveric specimen with soft tissue but required limited user interactions. In order to eliminate completely any manual intervention, we are currently working on a fully automatic contour extraction algorithm. The last limitation is about our validation study. The validation of the present approach, though successful, was only conducted on datasets of six dry bones and one cadaveric specimen with soft tissue. Thus, the results reported in this article are regarded still preliminary and more thorough validation study is needed before it can be transferred to clinical routine usage. Nonetheless, the experimental results from the present study demonstrated the accuracy and the robustness of the present approach.

ACKNOWLEDGMENTS

The author gratefully acknowledges the financial support from the Swiss Commission for Technology and Innovation (CTI/KTI) *via* project No. 13523.1 PFFLR-LS.

CONFLICT OF INTEREST

The authors have no conflict of interest related to this work.

ETHICAL STANDARDS

The medical research ethics committee of Inselspital, University of Bern, Switzerland, approved the cadaveric study.

REFERENCES

[1]Abdel-Aziz, Y., and H. Karara. Direct linear transformation from comparator coordinates into object space coordinates in close-range photogrammetry. In: Proceedings of ASP Symposium on Close-Range Photogrammetry, 1971, pp. 1–18.

[2]Aspert, N., D. Santa-Cruz, and T. Ebrahimi. Mesh: measuring errors between surfaces using the hausdorff distance. In: Proceedings of IEEE International Conference on Multimedia and Expo, Vol. 1, 2002, pp. 705–708.

[3]Barrett, W. A., and E. N. Mortensen. Interactive live-wire boundary extraction. *Med. Image Anal.* 1:331–341, 1997.

[4]Beaulé, P. E., E. Zaragoza, K. Motamedi, N. Copelan, and F. J. Dorey. Three-dimensional computed tomography of the hip in the assessment of femoroacetabular impingement. *J. Orthop. Res.* 23:1286–1292, 2005.

[5]Clohisy, J. C., J. C. Carlisle, P. E. Beaulé, Y.-J. Kim, R. T. Trousdale, R. J. Sierra, M. Leunig, P. L. Schoenecker, and M. B. Millis. A systematic approach to the plain radiographic evaluation of the young adult hip. *J. Bone Joint Surg. Am.* 90S(4):47–66, 2008.

[6]Duda, R., and P. Hart. Use of Hough transformation to detect lines and curves in pictures. *Commun. ACM* 15:11–15, 1972.

[7]Hartley, R., and A. Zisserman. Multiple View Geometry in Computer Vision (2nd ed.). Cambridge: Cambridge University Press, 2004.

[8]Heckbert, P. Graphics Gems IV. Oxford: Elsevier Ltd, pp. 474–485, 1994.

[9]Krekel, P. R., A. J. Vochteloo, R. M. Bloem, and R. G. Nelissen. Femoroacetabular impingement and its implications on range of motion: a case report. *J. Med. Case Rep.* 5:143, 2011.

[10]Lamecker, H., T. Wenckebach, and H. Hege. Atlas-based 3D shape reconstruction from X-ray images. In: Proceedings of 18th International Conference on Pattern Recognition, Vol. 1, 2006, pp. 371–374.

[11]Lewis, J. Fast normalized cross-correlation. *Vis. Interface* 10:120–123, 1995.

[12]Mitton, D., and K. Zhao. 3D reconstruction of the ribs from lateral and frontal X-rays in comparison to 3D CT-scan reconstruction. *J. Biomech.* 41:706–710, 2008.

[13]Pizer, S., E. Amburn, J. Austin, R. Cromartie, A. Geselowitz, T. Greer, B. Ter Haar Romeny, J. Zimmerman, and K. Zuiderveld. Adaptive histogram equalization and its variations. *Comput. Vis. Graph. Image Process.* 39:355–368, 1987.

[14]Sadowsky, O., G. Chintalapani, and R. Taylor. Deformable 2D–3D registration of the pelvis with a limited field of view, using shape statistics. *LNCS Springer* 4792:519–526, 2007.

[15]Schumann, S., X. Dong, M. Puls, L. P. Nolte, and G. Zheng. Calibration of C-arm for orthopedic interventions via statistical model-based distortion correction and robust phantom detection. In: ISBI, 2012, pp. 1204–1207.

[16]Schumann, S., M. Tannast, M. Bergmann, M. Thali, L. P. Nolte, and G. Zheng. A hierarchical strategy for reconstruction of 3D acetabular surface models from 2D calibrated X-ray images. *LNCS Springer* 7330:74–83, 2012.

[17]Schumann, S., M. Tannast, L. P. Nolte, and G. Zheng. Validation of statistical shape model reconstruction of the proximal femur—a morphology study. *Med. Eng. Phys.* 32:638–644, 2010.

[18]Tannast, M., D. Goricki, M. Beck, S. B. Murphy, and K. A. Siebenrock. Hip damage occurs at the zone of femoroacetabular impingement. *Clin. Orthop. Relat. Res.* 466: 273–280, 2008.
[19]Tannast, M., M. Kubiak-Langer, F. Langlotz, M. Puls, S. B. Murphy, and K. A. Siebenrock. Noninvasive three-dimensional assessment of femoroacetabular impingement. *J. Orthop. Res.* 25:122–131, 2007.
[20]Tannast, M., K. A. Siebenrock, and S. E. Anderson. Femoroacetabular impingement: radiographic diagnosis—what the radiologists should know. *AIH Am. J. Roentgenol.* 188:1540–1552, 2007.
[21]Vercauteren, T., X. Pennec, A. Perchant, and N. Ayache. Non-parametric diffeomorphic image registration with the demons algorithm. *LNCS Springer* 4792:319–326, 2007.
[22]Wicky, S., P. F. Blaser, C. H. Blanc, P. F. Leyvraz, P. Schnyder, and R. A. Meuli. Comparison between standard radiography and spiral CT with 3D reconstruction in the evaluation, classification and management of tibial plateau fractures. *Eur. Radiol.* 10:1227–1232, 2000.
[23]Yao, J., and R. Taylor. Assessing accuracy factors in deformable 2D/3D medical image registration using a statistical pelvis model. In: Proceedings of 9th International Conference on Computer Vision, Vol. 2, 2003, pp. 1329–1334.
[24]Zheng, G. Statistically deformable 2D/3D registration for estimating post-operative cup orientation from a single standard AP X-ray radiograph. *Ann. Biomed. Eng.* 38:2910–2927, 2010.
[25]Zheng, G., and S. Schumann. 3D reconstruction of a patient-specific surface model of the proximal femur from calibrated X-ray radiographs: a validation study. *Med. Phys.* 36:1155–1166, 2009.